Critical current density improvements in MgB_2 superconducting bulk samples by K_2CO_3 additions

Grivel, J.-C.

Published in:
Physica C: Superconductivity and its Applications

Link to article, DOI:
10.1016/j.physc.2018.03.012

Publication date:
2018

Document Version
Peer reviewed version

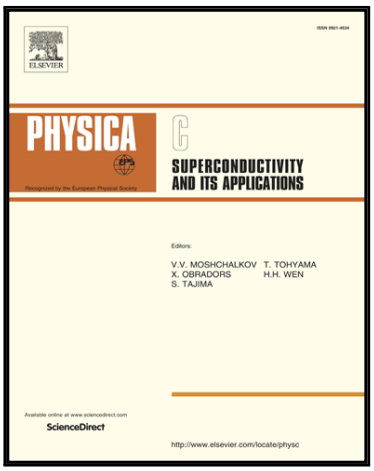

Critical current density improvements in MgB_2 superconducting bulk samples by K_2CO_3 additions

J.-C. Grivel

PII: S0921-4534(18)30111-4
DOI: 10.1016/j.physc.2018.03.012
Reference: PHYSC 1253329

To appear in: *Physica C: Superconductivity and its applications*

Received date: 6 March 2018
Accepted date: 28 March 2018

Please cite this article as: J.-C. Grivel , Critical current density improvements in MgB_2 superconducting bulk samples by K_2CO_3 additions, *Physica C: Superconductivity and its applications* (2018), doi: 10.1016/j.physc.2018.03.012

Critical current density improvements in MgB_2 superconducting bulk samples by K_2CO_3 additions

J.-C. Grivel*

Department of Energy Conversion and Storage, Technical University of Denmark, DK-4000 Roskilde, Denmark

Abstract

MgB_2 bulk samples with potassium carbonate doping were made by means of reaction of elemental Mg and B powders mixed with various amounts of K_2CO_3. The T_c of the superconducting phase as well as its a-axis parameter were decreased as a result of carbon doping. Potassium escaped the samples during reaction. The critical current density of MgB_2 was improved both in self field and under applied magnetic field for $T \leq 30$ K, with optimum results for 1 mol.% K_2CO_3 addition. The normalized flux pinning force (*f(b)*) shows that the flux pinning mechanism at low field is similar for all samples, following the predictions of the point pinning model. In contrast the behavior of *f(b)* is significantly altered at reduced fields (*b*) larger than unity by K_2CO_3 additions, tending towards surface pinning. Besides providing carbon, another effect of K_2CO_3 may originate from the presence of a transient liquid phase that appears to improve the crystallinity and thus the critical current density at low field.

Keywords: MgB_2; doping; carbon; potassium; K_2CO_3

***Corresponding author**

Email: jean@dtu.dk

Introduction

For several applications involving high magnetic fields such as magnets [1,2], energy storage devices [3,4], high power cables [5], etc., exploiting the superconducting properties of MgB_2 on a large-scale commercial level requires further improvements of the critical current density (j_c) performance of wires and bulk samples, because this parameter tends to be severely suppressed as soon as a magnetic field is acting on the material. This is especially important if MgB_2 is meant to be used at an operation temperature of 20 K. Besides the addition of nanoparticles acting as flux pinning centers [6-8], doping on the boron sites in the MgB_2 crystal lattice has been found to be effective in enhancing the pinning force and hence the j_c of MgB_2 under high magnetic fields [9-16]. It must however be underscored that only carbon substitution for boron results in improvements, whereas Al, the only other element able to substitute for B to a significant extent, induces adverse effects due to the different influence of these elements on H_{c2} [17-20]. Nevertheless, carbon doping generally results in a lowering of the j_c values under self-field and moderate applied magnetic field conditions [11-13]. For this reason, research activities are still ongoing in order to find ways of improving the j_c performance of MgB_2 samples at high magnetic fields without compromising their properties at lower fields. Among various possible categories of carbon source materials, metal carbonates are interesting as they may induce the formation of nanoparticles acting as additional flux pinning centers on top of the effect resulting from carbon incorporation in the MgB_2 lattice. Such studies have however only seldom been published. $SrCO_3$ additions were reported to induce a lowering of j_c, but this was for the ex-situ preparation route, i.e. adding $SrCO_3$ to pre-reacted MgB_2 powders [21]. In contrast, $CaCO_3$ produced from paper ash and added to a mixture of Mg and B powders to make MgB_2 via the in-situ route resulted in higher j_c values that were attributed to both carbon substitution and CaB_6 particles formation [22]. Ueda et al. [23] studied the effect of Na_2CO_3, an interesting option since Na doping in MgB_2 had been

theoretically studied as a way to increase the critical temperature (T_c) of MgB_2 [24]. A substantial improvement of the $j_c(B)$ performance was achieved in samples with $Mg_{1-2x}B_2(Na_2CO_3)_x$ compositions for $x \approx 0.055$, however most of the Na had left the samples.

The present work focused on testing the effect of K_2CO_3 additions on the formation and some superconducting properties of MgB_2. The melting point of K_2CO_3 (about 890°C) being higher than that of Na_2CO_3 (850°C), it could be expected that it has less tendency of leaving the samples by sublimation during processing. On the other hand, the effect of K doping in MgB_2 has not been the topic of extended research up to now. Since the heaviest alkaline elements (Rb and Cs) were reported to induce interesting effects on T_c [25], this was also an opportunity for looking for similar interactions between K and MgB_2.

Experimental details

As starting reagents, elemental powders consisting of Mg (Alfa Aesar, 99.8 % purity), amorphous boron (Aldrich, 95-97 %) and K_2CO_3 (Alfa Aesar, 99.997 %) were used. Since K_2CO_3 adsorbs humidity, it was dried at 300ºC for 24 h in air before being added to the other powders. Mixing was made with the following nominal ratios: $MgB_2 + xK_2CO_3$ ($0 \leq x \leq 4$ mol.%, with $\Delta x = 1$). A slight excess of B (2 at.%) was added to compensate for the impurities (including some Mg) present in the B commercial powder used for the present work [26]. Homogenising was conducted in a mechanical blender (Bachofen, type T2C). The mixed powders were then pressed into pellets with 12 mm diameter and 1.5 mm thickness under a pressure of 1.8 kbar. Heat treatment took place at 800°C for 1 h under Ar atmosphere for reacting the powders, with a heating rate of 100°C/h. Furnace cooling was used at the end of the treatment.

The sintered pellets were cut into three pieces with a diamond saw. One of them was crushed into powder and XRD patterns were recorded in a Bruker X-ray diffractometer with CuKα radiation (λ = 1.5406 Å) first without and then again with silicon powder (Alfa Aesar, 99.999%) mixed to the

powders as an internal standard for lattice parameters calculations performed using the UnitCell least square refinement programme [27]. The microstructure was studied by means of scanning electron microscopy (SEM) in a table-top TM3000 microscope from HITACHI equipped with a QUANTAX 70 EDS analyser, on another piece that was cast into epoxy resin and polished with abrasive suspensions down to 0.25 μm particle size. For magnetic measurements, 8.0 x 2.0 x 1.5 mm^3 bars were cut in the middle of the reacted pellets. The superconducting critical temperature (T_c) was determined as the mid-point of the diamagnetic transition measured by means of a vibrating sample magnetometer (VSM) in a CRYOGENIC Ltd Mini-CFMS under a magnetic field of 5 mT applied parallel to the longest axis of the samples in zero field conditions. For the evaluation of the critical current density (j_c), magnetisation hysteresis loops were recorded on the same samples still with the magnetic field parallel to the long axis and j_c was calculated using the Bean model. A differential thermal analysis (DTA) measurement was conducted on a 30 mg powder sample with 4 mol.% K_2CO_3 in a model STA 449C TG-DTA from Netzsch with a heating rate of 5 K/min up to 660°C under an argon flow of 40 ml/min. The crucibles consisted of alumina. α-Al_2O_3 powder (48 mg) was used as reference.

Results

The XRD patterns of the samples after reaction at 800ºC are shown in Fig.1. MgB_2 is clearly the majority phase in all samples. The only detectable impurity consists of MgO and the intensity of its reflections increases with the amount of K_2CO_3 in the starting composition. The lattice parameters calculated from the MgB_2 peak positions are listed in Table 1 and plotted in Fig.2. It appears that the a-axis parameter significantly decreases with increasing initial K_2CO_3 content, whereas the c-axis parameter only slightly increases. This behavior is typical for the effect of carbon doping on boron sites in the MgB_2 structure [11-13]. According to the relation established by Lee et al. [28] on the basis of a systematic study of C-substituted MgB_2 single crystals, the amount of carbon

introduced in the samples can be estimated as $MgB_{2-x}C_x$ with x equal to up to 0.04 in the sample with 4 mol.% K_2CO_3 addition. The x values for all samples are given in Table 1 (C_{XRD}). They are close to the expected results assuming full substitution of the nominal carbon content in the samples ("C_{nom}" in Table 1). The full width at half maximum (FWHM) of the MgB_2 (002) and (110) XRD peaks were evaluated using fits to a pseudo-Voigt function and are also presented in Table 1. Surprisingly, these values do not increase as soon as K_2CO_3 was present as would be expected considering the usual effect of carbon doping in MgB_2 [10,13]. Instead, they are first even slightly reduced and significantly increase only for the highest nominal K_2CO_3 content. This indicates that the crystallinity of MgB_2 first improves both in the ab-plane and along the c-axis for low K_2CO_3 additions, whereas the broadening effect of carbon substitution only becomes important at high concentrations.

In order to check if K doping might contribute to the a-axis lattice parameter variation and/or have a direct influence on the FWHM behavior, elemental analysis was performed by means of EDS on polished cross sections of the samples to assess the presence of potassium in the sintered samples. SEM images for all compositions are shown in Fig.3. The results of large area measurements (30000 μm^2) reveal that K is absent from all samples within the detection limit of the instrument (0.5 at.%), even in the case of 4 mol.% K_2CO_3 addition. This finding shows that potassium has been lost during the manufacturing process somehow similarly to the case of Na_2CO_3 doping, for which it was reported that most of the initial Na had left the samples [23]. It can thus be concluded that the decrease of the a-axis lattice parameter is not due to K doping, but is most probably resulting only from C substitution for B. Fig. 3f also shows that oxygen is mostly concentrated in large particles, which appear to consist primarily of MgO. These particles develop especially for the highest nominal K_2CO_3 contents. In contrast, B-rich magnesium boride particles, i.e. MgB_4, MgB_7 and MgB_{12} (pointed by arrows in Fig. 3f), do not grow significantly when the K_2CO_3 content increases.

Figure 4 shows the results of VSM magnetization measurements in zero field cooling mode in a DC field of 5 mT. The data were normalized to the magnetization value at 5 K. The temperature of the superconducting transition is obviously dependent on the K_2CO_3 initial content and decreases faster beyond 2 mol.% additions. This behavior is somehow reminiscent of that of the a-axis parameter. Referring again to the study of Lee et al. [28], the T_c variation of the present samples can be translated into carbon doping values, which are listed in Table 1 (C_{Tc}). These values are close to those estimated based on the a-axis parameter and therefore provide an additional indirect demonstration that carbon has been introduced into the MgB_2 lattice. By comparison with the carbon doping level that could be expected if all the carbon present in the initial K_2CO_3 powder had been substituting into MgB_2 (C_{nom} in Table 1), one can see again that K_2CO_3 is an efficient carbon source as nearly all carbon is stored into the superconductor. The overall reaction taking place in the powder mixture could be equivalent to:

$$Mg + 2B + xK_2CO_3 \rightarrow MgB_{2-x}C_x + xK_2O + O_2 \qquad (1)$$

Based on the XRD patterns, it can be deduced that at least a part of the released oxygen reacts with Mg, forming MgO. How far K_2O is present as a liquid phase (T_{melt} = 740°C) and evaporates as such or also maybe reacts with Mg according to: $Mg + K_2O \rightarrow MgO + 2K$ (2)

with further formation of MgO or decomposes into elemental potassium and oxygen on its own cannot easily be assessed due to the low initial amount of K_2CO_3 but in both cases, the transient presence of liquid potassium ($T_{melting}$ = 64ºC) or K_2O is likely to provide a flux or sintering aid improving the crystallinity of the MgB_2 grains so that the effect of carbon doping on the FWHM of the MgB_2 XRD peaks is cancelled for the lowest doping levels. Inhomogeneous distribution of carbon in MgB_2 tends to increase the superconducting transition width [29]. The suppression of ΔT_c

increase for low initial K_2CO_3 contents (Table 1) indeed indicates that the use of K_2CO_3 as a carbon source improves the homogeneity of carbon distribution in the MgB_2 matrix.

The $j_c(B)$ dependence calculated from magnetization hysteresis loops using the Bean model are shown in Fig.5 for measurements conducted at 30 K and 20 K. Similar plots for other measurement temperatures (i.e. 35 K, 25 K and 15 K) are shown in the supplementary files (Fig. S1). Close to T_c, j_c is lower in all samples treated with K_2CO_3, except for the 1 mol.% doped sample at low field, and systematically decreases with increasing nominal K_2CO_3 content. This can be due to the decrease of T_c. In contrast, at lower temperatures, the j_c of the samples that contained K_2CO_3 in their nominal composition tends to become relatively higher by comparison with the undoped sample. The highest self-field and low field j_c ($B \leq 2$ T) is observed in the $x = 0.01$ sample (1 mol. % K_2CO_3). However, the j_c of the undoped sample decreases slower than that of the others up to about 2.5 T, so that at 20 K, the K_2CO_3-free sample exhibits the highest j_c between 2.2 T and 2.9 T. nevertheless, at still higher fields, its performance is superseded again by those of the doped samples.

The pinning force calculated as $F_p = j_c \cdot B$, is plotted in Fig.6 for measurements performed at 30 K and 20 K. The $F_p(B)$ data for 35 K, 25 K and 15 K can be found in Fig.S2. The qualitative behavior of F_p closely follows that of j_c. At T close to T_c, F_p is larger in the undoped sample for the whole applied magnetic field range, but below 30 K F_p of the doped samples progressively becomes higher than without K_2CO_3 additions. However, it can be noted that the low field F_p of the samples with $x = 0.01$ and $x = 0.02$ K_2CO_3 additions at $T \leq 25$ K is anyway hardly larger than that of the pure sample in spite of a clear improvement of j_c in the field range. This suggests that the pinning force improvement only plays a marginal role in the improvement of j_c at relatively low applied magnetic fields.

In Fig.7, the normalized pinning force ($f = F_p/F_{p\,max}$) , which is the pinning force F_p normalized by the maximum value of F_p ($= F_{pmax}$) was plotted for all samples at 30 K and 20 K versus $b = B/B_{Fpmax}$ i.e. the applied magnetic field B normalized by the field corresponding to F_{pmax}. See Fig. S3 for the other measurement temperatures. The data are compared to the models corresponding to surface pinning (3), normal point pinning (4) and Δκ pinning (5) [30]:

$$f(b) = \frac{25}{16}\sqrt{b}\left(1-\frac{b}{5}\right)^2 \quad (3)$$

$$f(b) = \frac{9}{4}b\left(1-\frac{b}{3}\right)^2 \quad (4)$$

$$f(b) = 3b^2\left(1-\frac{2b}{3}\right) \quad (5)$$

For $b \leq 1$ the data for all samples show a similar dependence notwithstanding of temperature or composition. In this area, the shape of the experimental data tends to follow the point pinning model. Nevertheless, since the experimental curves lie between the point pinning and Δκ pinning, it can be assumed that the latter mechanism also plays a role. At higher reduced fields however, the samples that contained K_2CO_3 in their nominal composition show a systematic deviation towards a f(b) dependence closer to that predicted for surface pinning, whereas the undoped sample still exhibits a behavior close to the theoretical predictions of the point pinning model. This is observed for all investigated temperatures from 15 K to 35 K as shown also in the supplementary files (Fig S3). Such a behavior is typical for the effect of carbon doping in MgB_2, as was shown by Wang et al. [31]. Other reports demonstrating a dominant surface pinning mechanism under high magnetic fields consecutive to carbon doping have been published, e.g. Ghorbani et al. [32] for succinic acid

additions, while several publications dealing with carbon doping show an upwards deviation of f(b) upon doping without necessarily relating this effect to a specific pinning mechanism [16,23,34].

It is clear that K_2CO_3 additions only have an effect on the dominant flux pinning mechanism acting at high fields. The observed modification can be ascribed to carbon doping into the MgB_2 lattice. On the other hand, the j_c improvements under self-field and up to the field corresponding to the maximum pinning force (*f(b)* = 1) do not originate from modifications of the flux pinning mechanism. Instead, this enhancement is more likely due to a higher homogeneity and/or crystallinity reflected in lower ΔT_c and FWHM values observed up to $x \approx 0.03$.

Figure 8 shows a detail of the DTA trace of the initial powder mixture containing 4 mol.% K_2CO_3. While the sharp endothermic peak due to Mg melting is clearly visible close to 650°C, a broader endothermic event is registered from 605°C as a prominent shoulder prior to Mg melting. Such a feature is not normally present in undoped Mg-2B powder mixtures [34] and most probably reflects a reaction between K_2CO_3 and at least one of the other two components (Mg and B) of the mixture. This can explain why K_2CO_3 is no more present in the samples after heat treatment at 800°C, whereas K_2CO_3 would otherwise be stable up to 890°C. These observations also reveal that the effect of K_2CO_3 is different from that of some metallic elements, which merely induce a lowering of the melting temperature of Mg as a result of a simple eutectic reaction [35-42].

Conclusions

K_2CO_3 was found to be an efficient carbon source for doping in MgB_2 with a close to 100% transfer of the carbon atoms from K_2CO_3 to the MgB_2 lattice. Interestingly, the full width at half maximum of the MgB_2 X-ray diffraction peaks goes through a minimum for 1 – 2 mol.% K_2CO_3 addition. Reduced lattice strain and/or slightly larger mosaic grains in the MgB_2 crystallites could contribute to this effect. The transient presence of liquid potassium, although not ascertained, could

be responsible for this effect. Although the flux pinning mechanism at low reduced fields is not modified by the use of K_2CO_3, j_c is improved under low and self-field conditions for $T \leq 30$ K, especially for the addition of 1 mol.% K_2CO_3. Contrary to carbon and oxygen (forming MgO), which remain in the samples, potassium was no more detected after reaction. It could be interesting to test K_2CO_3 additions in MgB_2 wires to check whether the self-field critical current is also improved or if the confined environment, likely to help retaining potassium in the samples, would lead to different effects.

Acknowledgements

Mr. Henrik Paulsen is gratefully acknowledged for preparing the polished cross-sections of the samples for SEM investigations.

References

[1] D.A. Abin, N.A. Mineev, M.A. Osipov, S.V. Pokrovskii and I.A. Rudnev, Dry cryomagnetic system with MgB_2 coil, J, Phys. Conf. Ser. 941 (2017) 012056

[2] J. Liu, H. Ma, L. Huang and P. Ju, Research on an axial Maglev device with primary superconductive coils for a 1000 MW hydraulic generator set, IEEE Trans. Appl. Supercond. 27 (2017) 5000106

[3] S. Mizuno, T. Yagai, T. Okubo, S. Mizuochi, M. Kamibayashi, M. Jinbo, T. Takao, Y. Makida, T. Shintomi, N. Hirano, T. Komagome, K. Tsukada, Y. Onji, Y. Arai, M. Tomita, D. Miyagi, M. Tsuda and T. Hamajima, Feasibility study of MgB_2 cable for pancake coil of energy storage device, IEEE Trans. Appl. Supercond. Accepted for publication, DOI 10.1109/TASC.2018.2794334

[4] A. Morandi, A. Anemona, G. Angeli, M. Breschi, A. Della Corte, C. Ferdeghini, C. Gandolfi, G. Grandi, G. Grasso, L. Martini, U. Melaccio, D. Nardelli, P.L. Ribani, S. Siri, M. Troppeano, S. Turtù and M. Vignolo, The DRYSMES4GRID project: Development of a 500 kJ/200 kW cryogen-free cooled SMES demonstrator based on MgB_2, IEEE Trans. Appl. Supercond. 28 (2018) 5700205

[5] K. Konstantopoulou, A. Ballarino, A. Gharib, A. Stimac, M. Garcia Gonzalez, A.T. Perez Fontenla and M. Sugano, Electro-mechanical characterization of MgB_2 wires for the superconducting link project at CERN, Supercond. Sci. Technol. 29 (2016) 084005

[6] J. Wang, Y. Bugoslavsky, A. Berenov, L. Cowey, A.D. Caplin, L.F. Cohen, L.D. Cooley, X. Song and D.C. Larbalestier, High critical current density and improved irreversibility field in bulk MgB_2 made by a scalable, nanoparticle addition route, Appl. Phys. Lett. 81 (2002) 2026 - 2028

[7] E. Babic, N. Novosel, D. Pajic, S. Galic, K. Zadro and D. Drobac, Magnetic nanoparticles in MgB_2: vortex pinning, pair breaking and connectivity, J. Magn. Magn. Mater. 400 (2016) 88 – 92

[8] N. Novosel, S. Galic, D. Pajic, K. Zadro and E. Babic, Enhancing superconducting properties of MgB_2 by addition of magnetic particles, J. Supercond. Nov. Magn. 28 (2015) 425 – 430

[9] M.G. Babaoglu, S. Safran, Ö.Civek, H. Ail, E. Ertekin, Md. Shahriar, A. Hossein, E. Yanmaz and A. Gencer, Microstructural and superconducting properties of C_6H_6 added bulk MgB_2 superconductor, J. Magn. Magn. Mater. 324 (2012) 3455 – 3459

[10] S.X. Dou, O. Shcherbakova, W.K. Yeoh, J.H. Kim, S. Soltanian, X.L. Wang, C. Senatore, R. Flükiger, M. Dhalle, O. Husnjak and E. Babic, Mechanism of enhancement in electromagnetic properties of MgB_2 by nano SiC doping, Phys. Rev. Lett. 98 (2007) 097002

[11] S. Soltanian, J. Horvat, X.L. Wang, P. Munroe and S.X. Dou, Effect of nano-carbon particle doping on the flux pinning properties of MgB_2 superconductor, Physica C 390 (2003) 185 – 190

[12] C.H. Cheng, H. Zhang, Y. Zhao, Y. Feng, X.F. Rui, P. Munroe, H.M. Zeng, N. Koshizuka and M. Murakami, Doping effect of nano-diamond on superconductivity and flux pinning in MgB_2, Supercond. Sci. Technol. 16 (2003) 1182 – 1186

[13] J.M. Parakkandy, M. Shahabuddin, M. Shahabuddin Shah, N.S. Alzayed, S.A.S. Qaid, N.M. Ramay and M.A. Shar, Effect of glucose doping on the MgB_2 superconductors using cheap crystalline boron, Physica C 519 (2015) 137 – 141

[14] L.B.S. Da Silva, A.A. Vianna, A.L.R. Manesco, E.E. Hellstrom and D. Rodrigues Jr., The influence of stearic acid addition on the superconducting properties of MgB_2, IEEE Trans. Appl. Supercond. 26 (2016) 7100204

[15] J.H. Kim, S.X. Dou, M.S.A. Hossain, X. Xu, J.L. Wang, D.Q. Shi, T. Nakane and H. Kumakura, Systematic study of a MgB_2 + $C_4H_6O_5$ superconductor prepared by the chemical solution route, Supercond. Sci. Technol. 20 (2007) 715 - 719

[16] Z. Gao, Y. Ma, X. Zhang, D. Wang, Z. Yu, K. Watanabe, H. Yang and H. Wen, Strongly enhanced critical current density in MgB_2/Fe tapes by stearic acid and stearate doping, Supercond. Sci. Technol. 20 (2007) 485 - 489

[17] B. Kang, M.-S. Park, H.-S. Lee, M.-H. Jung and S.-I. Lee, Comparison between Al and C substitutions in the upper critical field of MgB_2 single crystals, J. Kor. Phys. Soc. 58 (2011) 498 - 502

[18] J.Y. Xiang, D.N. Zheng, J.Q. Li, S.L Li, H.H Wen and Z.X.Zhao, Effects of Al doping on the superconducting and structural properties of MgB_2, Physica C 386 (2003) 611-615

[19] G.J. Xu, J.-C. Grivel, A.B Abrahamsen, X.P. Chen and N.H. Andersen, Structure and superconductivity of double-doped $Mg_{1-x}(Al_{0.5}Li_{0.5})_xB_2$, Physica C 399 (2003) 8-14

[20] G.J. Xu, J.-C. Grivel, A.B Abrahamsen, X.P. Chen and N.H. Andersen, Superconducting properties of Zn and Al double-doped $Mg_{1-x}(Zn_{0.5}Al_{0.5})_xB_2$, Physica C 403(2004) 113-118

[21] P. Kováč, I. Hušek, T. Melišek, C.R.M. Grovenor, S. Haigh and H. Jones, Improvement of the current carrying capability of ex-situ MgB_2 wires by normal particle additions, Supercond. Sci. Technol. 17 (2004) 1225 - 1230

[22] K.S. Tan, S.K. Chen, B.H. Jun and C.J. Kim, Enhancement in critical current density and irreversibility field of bulk MgB_2 by C and $CaCO_3$ co-addition, Supercond. Sci. Technol. 21 (2008) 105013

[23] S. Ueda, J.-I. Shimoyama, A. Yamamoto, S. Horii and K. Kishio, Enhanced critical current properties observed in Na_2CO_3-doped MgB_2, Supercond. Sci. Technol. 17 (2004) 926 – 930

[24] N.I. Medvedeva, A.L. Ivanovskii, J.E. Medvedeva and A.J. Freeman, Electronic structure of superconducting MgB_2 and related binary and ternary borides, Phys. Rev. B 64 (2001) 020502

[25] A.V. Palnichenko, O.M. Vyaselev and N.S. Sidorov, Influence of Rb, Cs, and Ba on the superconductivity of magnesium diboride, JETP Letters 86 (2007) 272 – 274

[26] J.C. Grivel, A. Alexiou, K. Rubešová, X. Tang, N.H. Andersen, M. von Zimmermann and A. Watenphul, Preparation and characterization of $Mg_{1-x}B_2$ bulk samples and Cu/Nb sheathed wires with low grade amorphous boron powder, J. Supercond. Nov. Magn. 27 (2014) 497-504

[27] T.J.B. Holland and S.A.T. Redfern, Unit cell refinement from powder diffraction data: The use of regression diagnostics, Mineral. Mag., 61 (1997) 65-77.

[28] S. Lee, M. Takahiko, A. Yamamoto, H. Uchiyama and S. Tajima, Carbon-substituted MgB_2 single crystals, Physica C 397 (2003) 7 – 13

[29] C. Senatore, P. Lezza, R. Lortz, O. Shcherbakova, W.K. Yeoh, S.X. Dou and R. Flükiger, Specific heat and magnetic relaxation analysis of MgB_2 bulk samples with and without additives, IEEE Trans. Appl. Supercond. 17 (2007) 2941 – 2944

[30] T. Goto, K. Inagaki and K. Watanabe, Critical current density in filamentary (Nd, Sm, Eu, Gd) – Ba – Cu – O superconductors prepared by a solution spinning method, Physica C 330 (2000) 51 – 57

[31] J.L. Wang, R. Zeng, J.J. Kim, L. Lu and S.X. Dou, Effects of C substitution on the pinning mechanism of MgB_2, Phys. Rev. B 77 (2008) 174501

[32] S.R. Ghorbani, M. Darini, X.L. Wang, M.S.A. Hossain and S.X. Dou, Vortex flux pinning mechanism and enhancement of in-field j_c in succinic acid doped MgB_2, Sol. State Commum. 168 (2013) 1 - 5

[33] C.D. Wang, D.L. Wang, X.P. Zhang, C. Yao, C.L. Wang and Y.W. Ma, Aniline doping and high energy milling to greatly enhance electromagnetic properties of magnesium diboride superconductors, Physica C 489 (2013) 36 - 39

[34] J.C. Grivel and M. Burdusel, Preparation and characterization of Sc doped MgB_2 wires, Physica C 528 (2016) 65 - 72

[35] Y. Hishinuma, A. Kikuchi, K. Matsuda, K. Nishimura, Y. Kubota, S. Hata, S. Yamada and T. Takeuchi, Microstructure and superconducting properties of Cu addition MgB_2 multifilamentary wires using boron isotope powder as the boron source material, Physics Procedia 36 (2012) 1486-1491

[36] J.-C. Grivel, Attempts at doping indium in MgB_2, Physica C 531 (2016) 67 - 71

[37] P. Badica, G. Aldica, M. Burdusel and K. Endo, Composites of MgB_2 with Bi_2O_3, Bi, Sb_2O_3, or Sb obtained by ex-situ spark plasma sintering, Jpn. J. Appl. Phys. 51 (2012) 11PG13

[38] D. Batalu, G. Aldica, S. Popa, L. Miu, M. Enculescu, R.F. Negrea, I. Pasuk and P. Badica, High magnetic field enhancement of the critical current density by Ge, GeO_2 and $Ge_2C_6H_{10}O_7$ additions to MgB_2, Scripta Materialia 82 (2014) 61 – 64

[39] J. Huo, Y.C. Liu, Z.Z. Dong and H. Jiang, Effect of Sn-doping on the sintering process of MgB_2 and its superconductive properties, J. Mater. Sci. Mater. Electron. 22 (2011) 233 – 237

[40] M. Kuhberger and G. Gritzner, Effects of Sn, Co and Fe on MgB_2, Physica C 370 (2002) 39 - 43

[41] J.-C. Grivel, A. Abrahamsen and J. Bednarčik, Effects of Cu or Ag additions on the kinetics of MgB_2 phase formation in Fe-sheathed wires, Supercond. Sci. Technol. 21 (2008) 035006

[42] J.-C. Grivel, N.H. Andersen, P.G.A.P. Pallewatta, Y. Zhao and M.v. Zimmermann, Influence of Bi, Se and Te additions on the formation temperature of MgB_2, Supercond. Sci. Technol. 25 (2012) 015010

Figure captions

Figure 1: XRD patterns of the samples after reaction at 800ºC. The nominal K_2CO_3 content is indicated in mol.% above the respective patterns. The Miller indices denote MgB_2 diffraction peaks. ● : MgO.

Figure 2: Lattice parameters of the MgB_2 phase versus nominal K_2CO_3 content.

Figure 3: SEM images (backscattering mode) of polished cross-sections of the samples with nominal K_2CO_3 contents equal to 0 mol. % (a); 1 mol. % (b); 2 mol. % (c), 3 mol. % (d) and 4 mol. % (e) after reaction at 800°C. (f): EDS map showing the distribution of oxygen (green in online version) in the sample with 4 mol. % nominal K_2CO_3 content. The same magnification was used for all images. The arrows in (a) and (e) point towards boron-rich magnesium boride grains.

Figure 4: VSM data showing the superconducting transition in reacted samples with various nominal K_2CO_3 contents: 0 mol.% (a), 1 mol.% (b), 2 mol.% (c), 3 mol.% (d), 4 mol.% (e). Inset, T_c versus K_2CO_3 initial content.

Figure 5: Critical current density (j_c) at 30 K and 20 K versus applied magnetic field (B) calculated with the Bean model using magnetization hysteresis loops. The nominal K_2CO_3 content is indicated as x in $MgB_{2-x}C_x$ equivalent composition.

Figure 6: Pinning force (F_p) at 30 K and 20 K versus applied magnetic field (B) for samples with various nominal K_2CO_3 contents expressed as x in $MgB_{2-x}C_x$ equivalent composition.

Figure 7: Normalized pinning force $f = F_p/F_{pmax}$ at 30 K and 20 K versus the normalized magnetic field $b = B/B_{Fpmax}$. The data for the different nominal K_2CO_3 contents expressed as x in $MgB_{2-x}C_x$ equivalent composition, are compared to theoretical predictions of three flux pinning mechanism models: surface pinning (S), point pinning (P) and $\Delta\kappa$ pinning (K).

Figure 8: DTA trace recorded on the initial Mg + 2B + 4 mol.% K_2CO_3 powder mixture with a heating rate of 5 °C/min in Ar.

Table captions

Table 1: *a*-axis and *c*-axis lattice parameters; critical temperature (T_c) and transition width (ΔT_c) (10% - 90% of the maximum diamagnetic signal); full width at half maximum (FWHM) of the MgB_2 (002) and (110) X-ray diffraction peaks; carbon content estimated from XRD data (C_{XRD}) and T_c values (C_{Tc}) as well as theoretical maximum carbon doping level (C_{nom}) of the MgB_2 + xK_2CO_3 samples after heat treatment at 800°C.

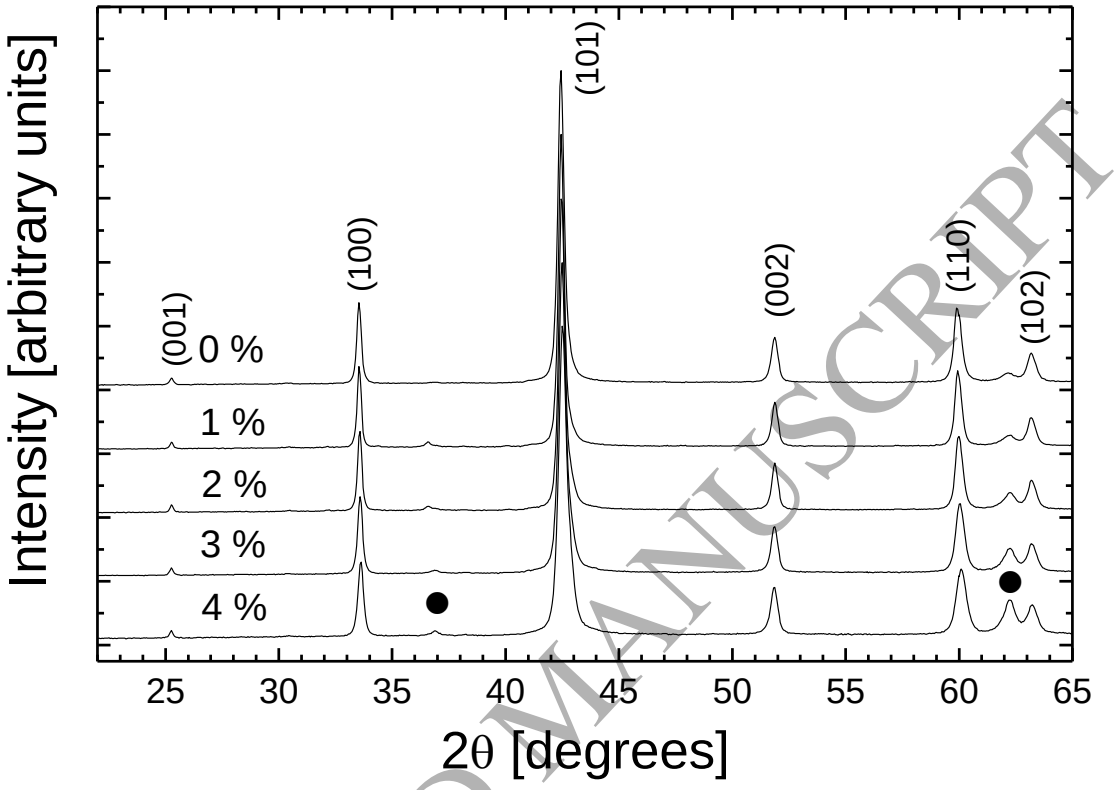

Figure 1

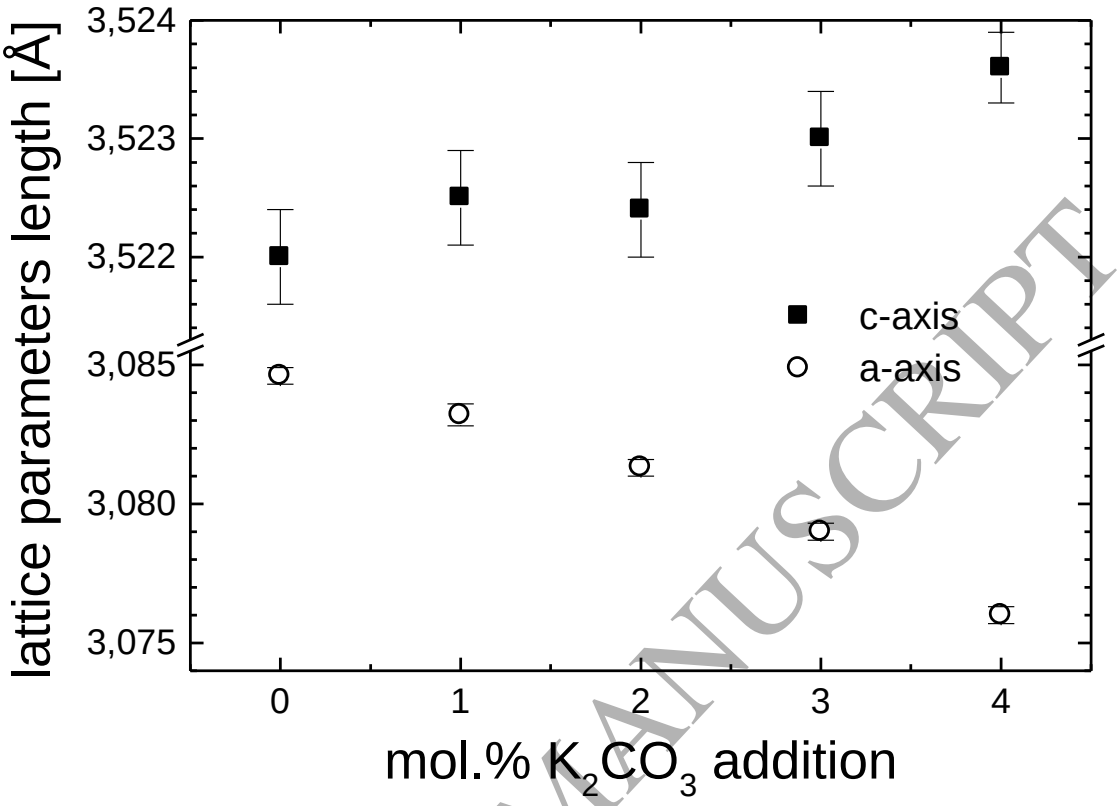

Figure 2

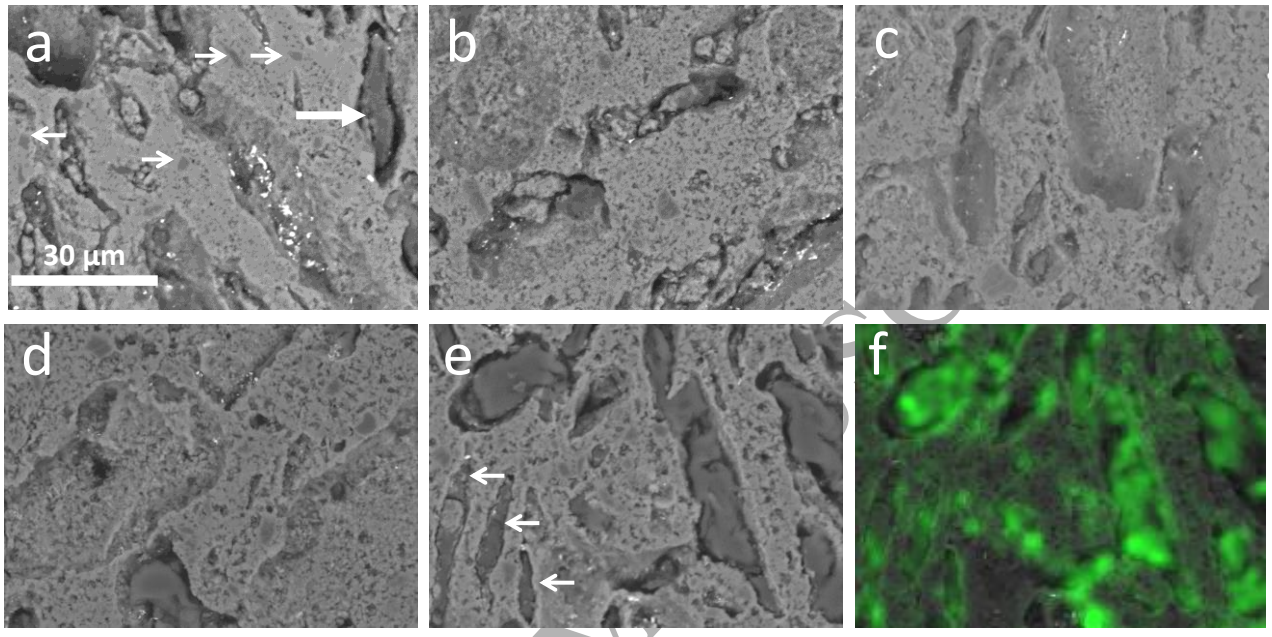

Figure 3

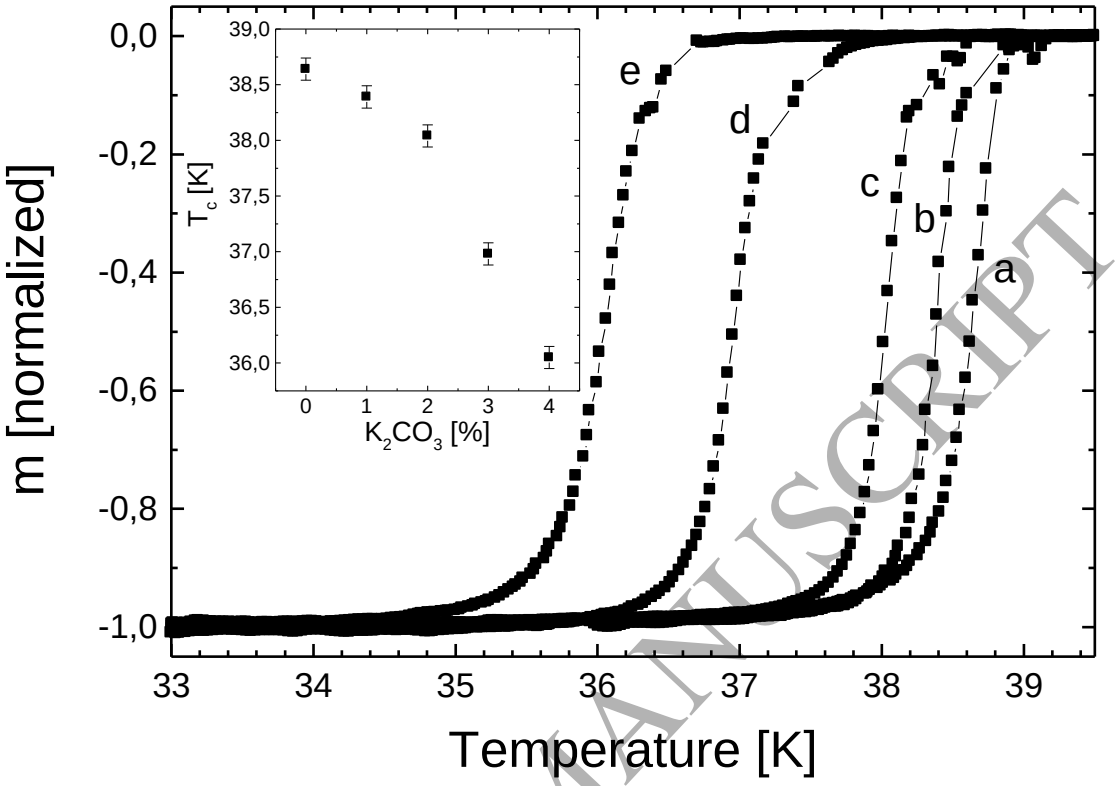

Figure 4

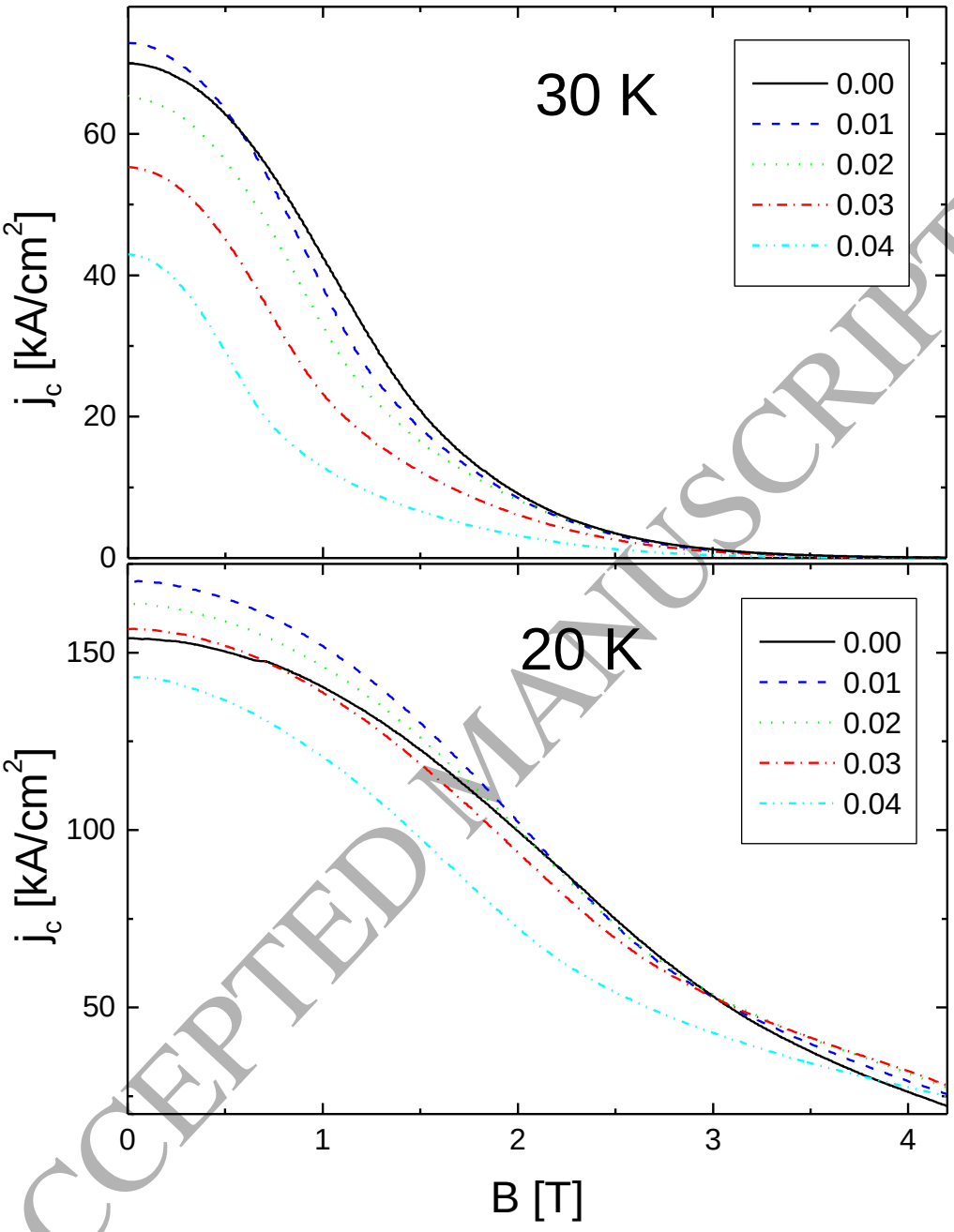

Figure 5

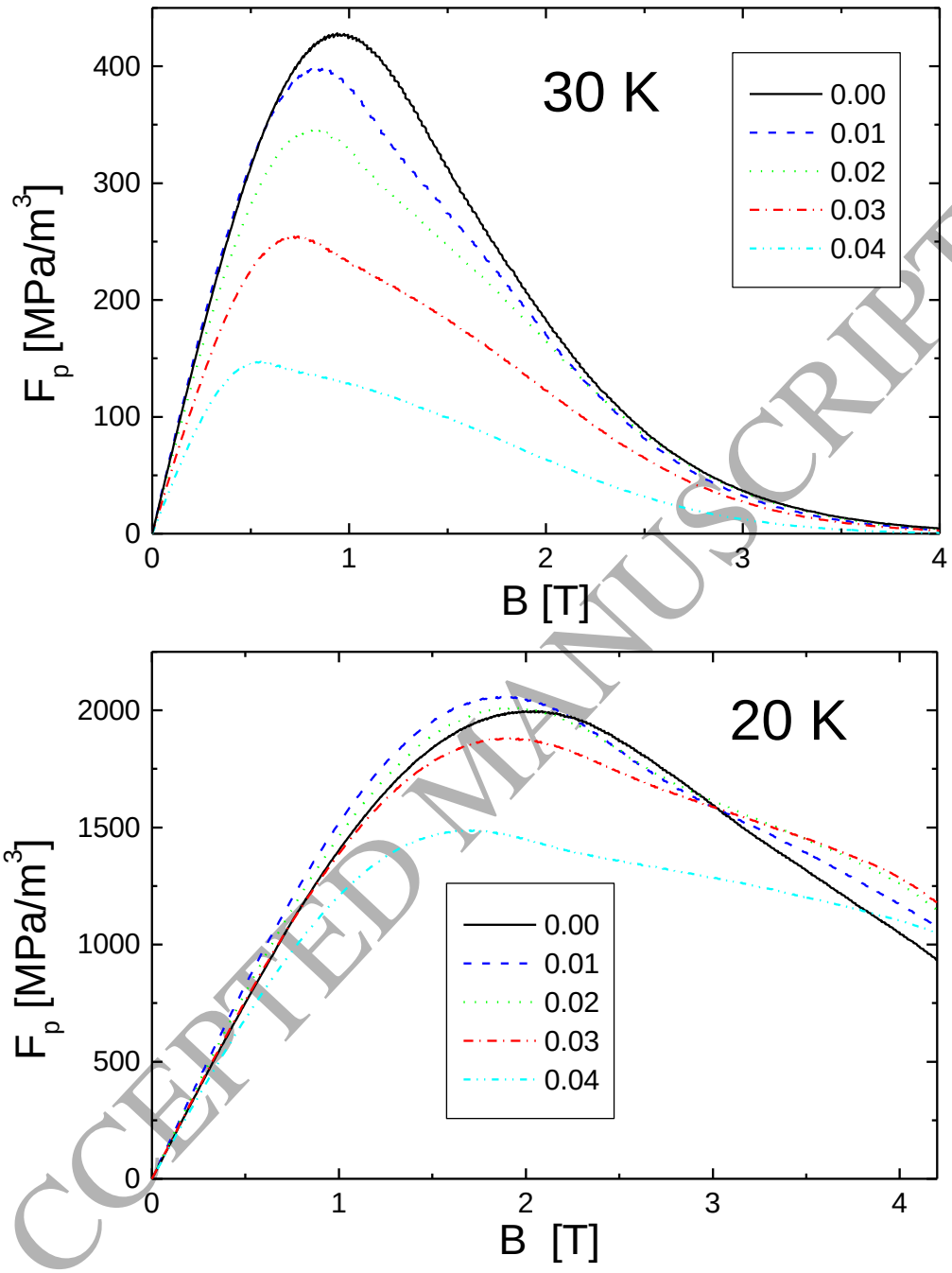

Figure 6

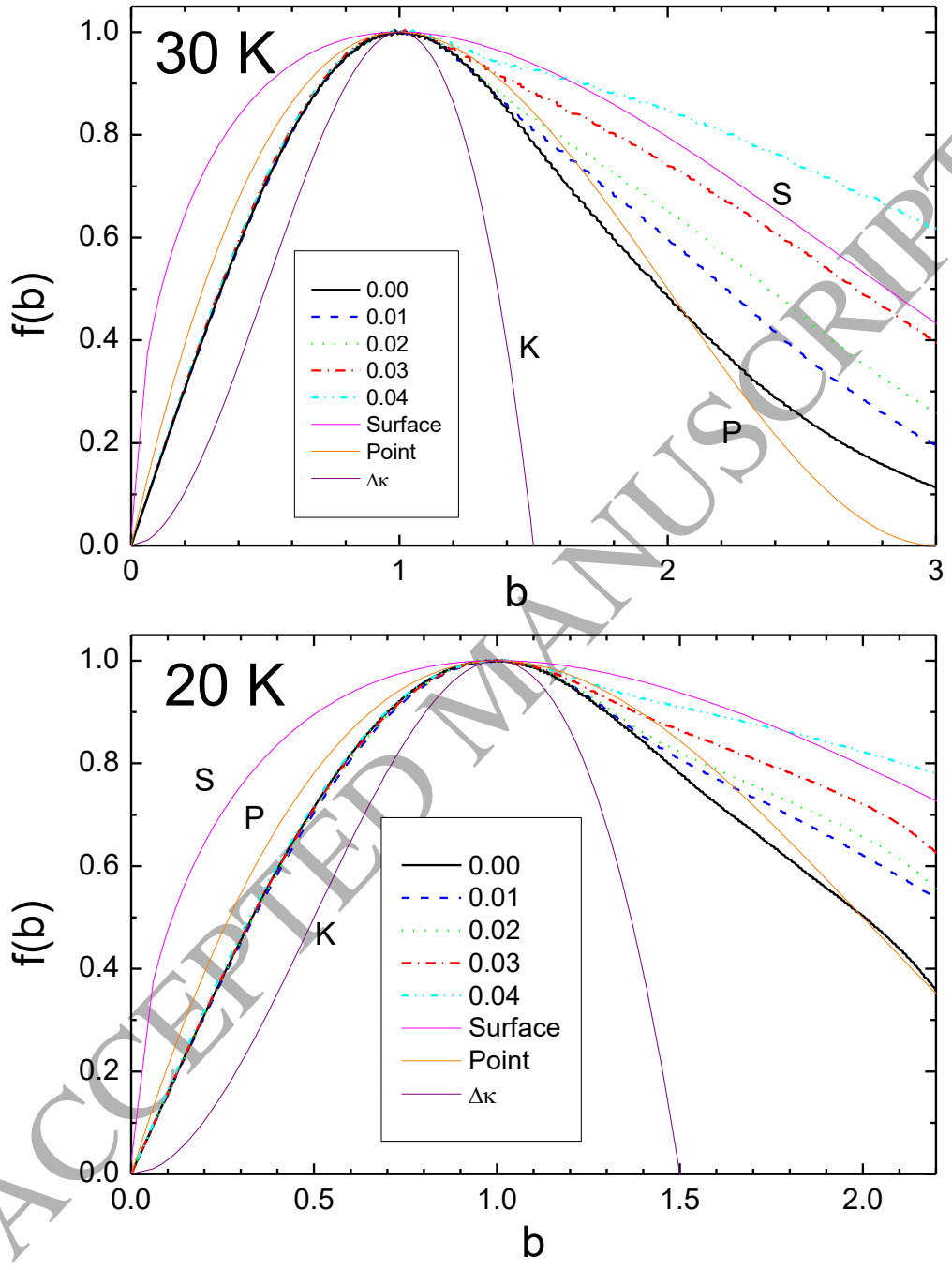

Figure 7

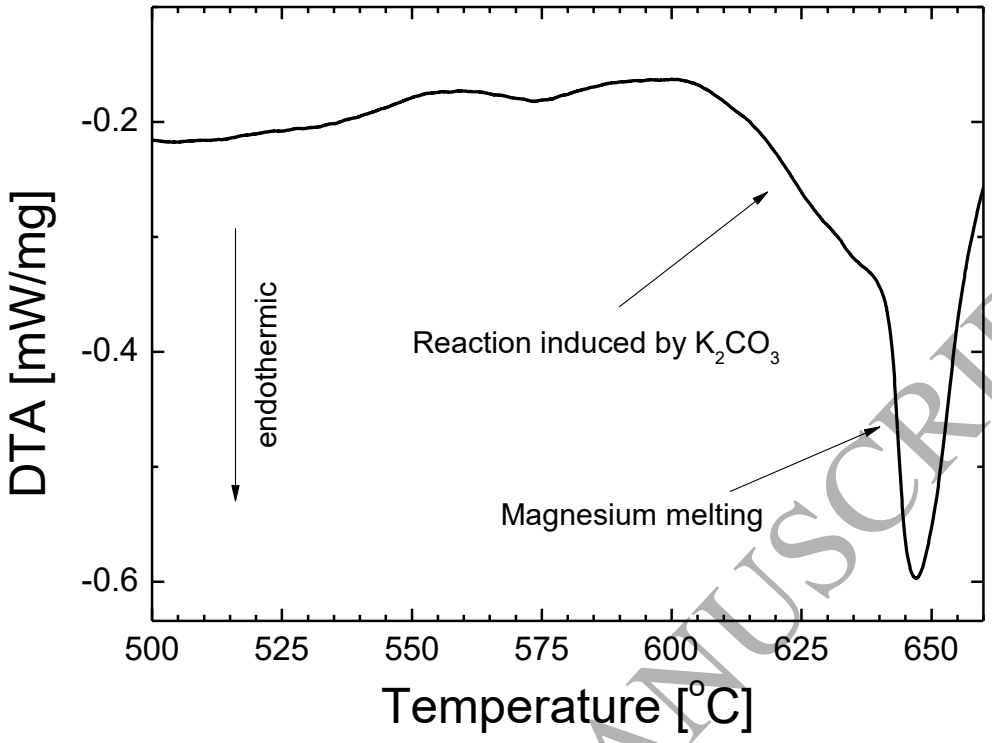

Figure 8

Nominal K_2CO_3	a	c	T_c	ΔT_c	$FWHM_{(002)}$	$FWHM_{(110)}$	C_{XRD}	C_{Tc}	C_{nom}
[mol.%]	[Å]	[Å]	[K]	[K]	[°] (2θ)	[°] (2θ)	[Expressed as x in $MgB_{2-x}C_x$]		
0	3.0846(3)	3.5220(4)	38.64(8)	0.61(9)	0.310(6)	0.365(7)	0.000	0.000	0.000
1	3.0832(4)	3.5225(4)	38.39(8)	0.55(9)	0.289(5)	0.324(6)	0.008(3)	0.004(2)	0.010
2	3.0813(3)	3.5224(4)	38.04(8)	0.59(9)	0.290(5)	0.345(7)	0.016(3)	0.008(3)	0.020
3	3.0790(3)	3.5230(4)	36.98(8)	0.79(9)	0.317(6)	0.398(7)	0.028(3)	0.024(4)	0.030
4	3.0760(3)	3.5236(3)	36.05(8)	0.83(9)	0.336(7)	0.472(8)	0.040(3)	0.036(4)	0.040

Table 1

Supplementary files

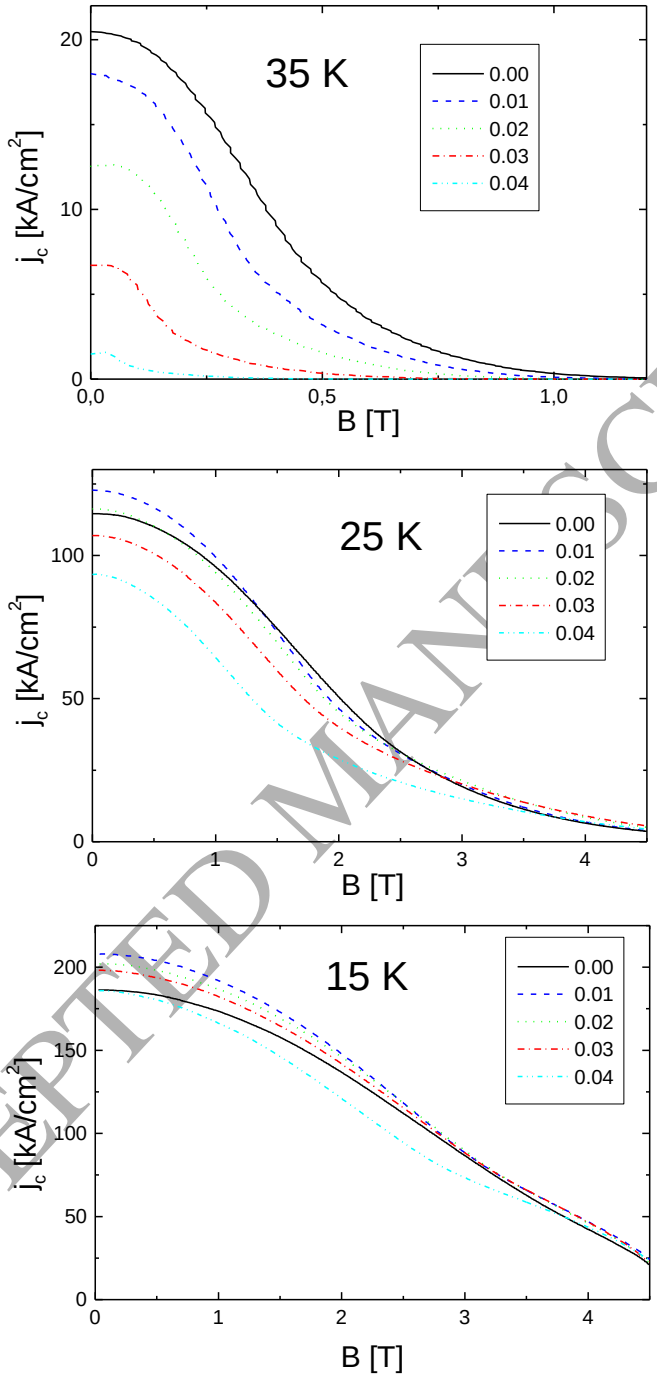

Figure S1: Critical current density (j_c) at 35 K, 25 K and 15 K versus applied magnetic field (B) calculated with the Bean model using magnetization hysteresis loops. The nominal K_2CO_3 content is indicated as x in $MgB_{2-x}C_x$ equivalent composition.

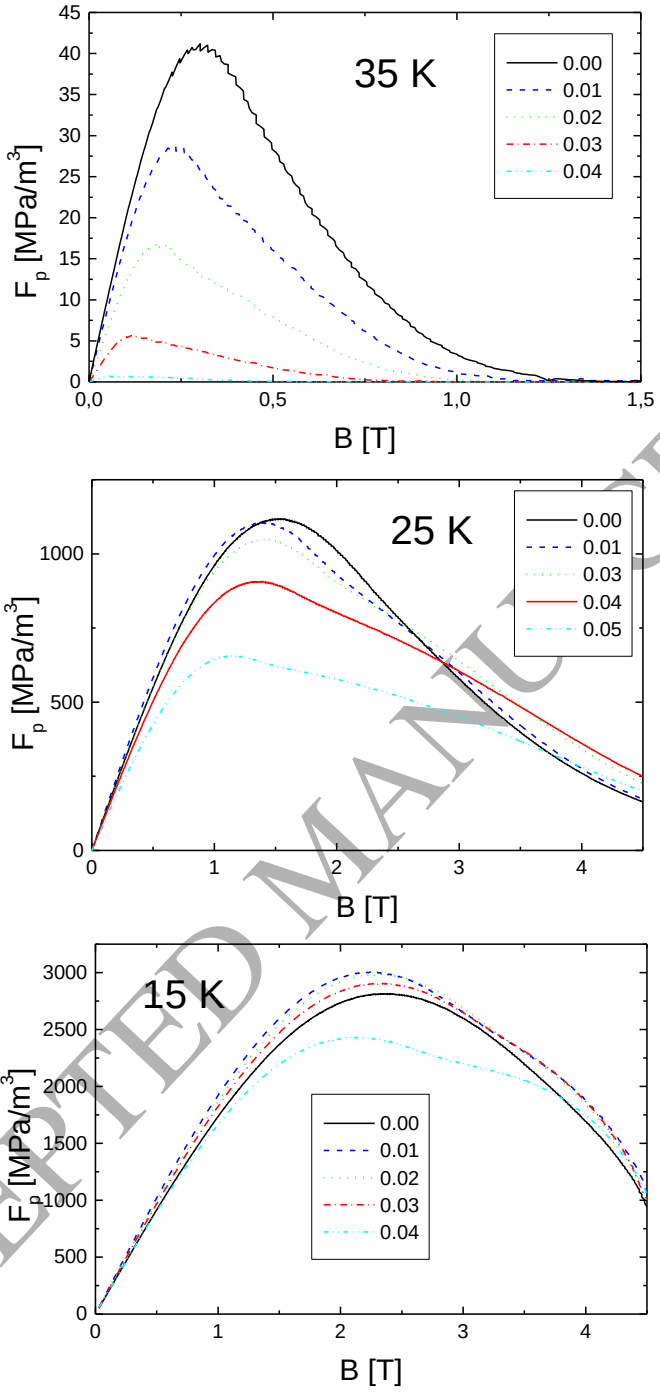

Figure S2: Pinning force (F_p) at 35 K, 25 K and 15 K versus applied magnetic field (B) for samples with various nominal K_2CO_3 contents expressed as x in $MgB_{2-x}C_x$ equivalent composition.

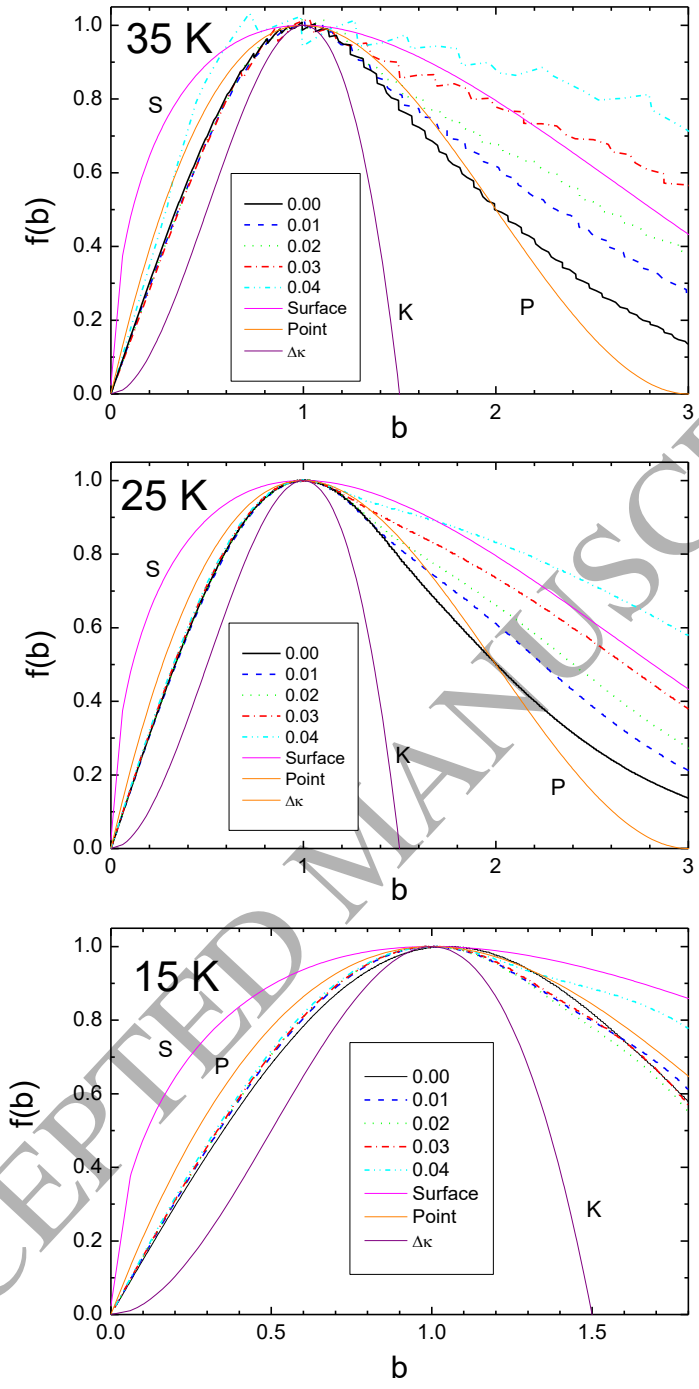

Figure S3: Normalized pinning force f = F_p/F_{pmax} at 35 K, 25 K and 15 K versus the normalized magnetic field b = B/B_{Fpmax}. The data for the different nominal K_2CO_3 contents expressed as x in $MgB_{2-x}C_x$ equivalent composition are compared to theoretical predictions of three flux pinning mechanism models: surface pinning (S), point pinning (P) and Δκ pinning (K).